Microfluid Nanofluid (2016) 20:165
DOI 10.1007/s10404-016-1828-9

RESEARCH PAPER

Engineering droplet navigation through tertiary-junction microchannels

M. Baig[1] · S. Jain[1] · S. Gupta[1] · G. Vignesh[1] · V. Singh[1] · S. Kondaraju[2] · S. Gupta[1]

Received: 25 July 2016 / Accepted: 8 November 2016 / Published online: 26 November 2016

Abstract We present an experimental and in silico investigation of path selection by a single droplet inside a tertiary-junction microchannel using oil-in-water as a model system. The droplet was generated at a T-junction inside a microfluidic chip, and its flow behavior as a function of droplet size, streamline position, viscosity, and Reynolds number (*Re*) of the continuous phase was studied downstream at a tertiary junction having perpendicular channels of uniform square cross section and internal fluidic resistance proportional to their lengths. Numerical studies were performed using the multicomponent lattice Boltzmann method. Both the experimental and numerical results showed good agreement and suggested that at higher *Re* equal to 3, the flow was dominated by inertial forces resulting in the droplets choosing a path based on their center position in the flow streamline. At lower *Re* of 0.3, the streamline-assisted path selection became viscous force-assisted above a critical droplet size. As the *Re* was further reduced to 0.03, or when the viscosity of the dispersed phase was increased, the critical droplet size for transition also decreased. This multivariate approach can in future be used to engineer sorting of cells, e.g., circulating tumor cells (CTCs) allowing early-stage detection of life-threatening diseases.

Keywords Tertiary-junction · Droplet microfluidics · Droplet sorting · Lattice-Boltzmann · Path selection

1 Introduction

Droplet microfluidics has greatly evolved in the past two decades with researchers demonstrating ingenious strategies for droplet manipulation (Velev et al. 2003), generation (Glawdel et al. 2012; Christopher et al. 2008; Sang et al. 2009; Husny and Cooper-White 2006; Liu and Zhang 2009; Xu et al. 2008; Garstecki et al. 2006), sorting (Teh et al. 2008; Tan et al. 2008), trapping (Huebner et al. 2009; Doh et al. 2012), merging (Baroud et al. 2010; Niu et al. 2008) and splitting (Link et al. 2004) operations in complex microfluidic networks. These studies involve the use of either internal forces such as interfacial tension, viscous drag, inertial, lift and centripetal forces (Xu et al. 2008; Garstecki et al. 2006; Teh et al. 2008; Tan et al. 2008) to control liquid droplet movement or the application of external fields (magnetic, electrical, optical etc.) to engineer microdroplet mobility (Zakinyan et al. 2012; Mugele et al. 2010; Lee 2013). Literature suggests that the path chosen by a droplet in a symmetric binary junction microchannel depends on the global architecture of the microfluidic network (Tan et al. 2004; Choi et al. 2011; Schindler and Ajdari 2008; Sessoms et al. 2009; Jousse et al. 2006; Belloul et al. 2011; Bruus 2007) (assuming complete droplet slip at the walls) analogous to the Kirchhoff's law for current flow in an electrical circuit. This means that the volumetric flow rate of the continuous phase carrying the droplet is the highest in the path having the least resistance. For

Electronic supplementary material The online version of this article (doi:10.1007/s10404-016-1828-9) contains supplementary material, which is available to authorized users.

✉ S. Gupta
shalinig@chemical.iitd.ac.in

[1] Department of Chemical Engineering, Indian Institute of Technology Delhi, Hauz Khas, New Delhi 110016, India

[2] School of Mechanical Sciences, Indian Institute of Technology Bhubaneswar, Bhubaneswar, Odisha 751013, India

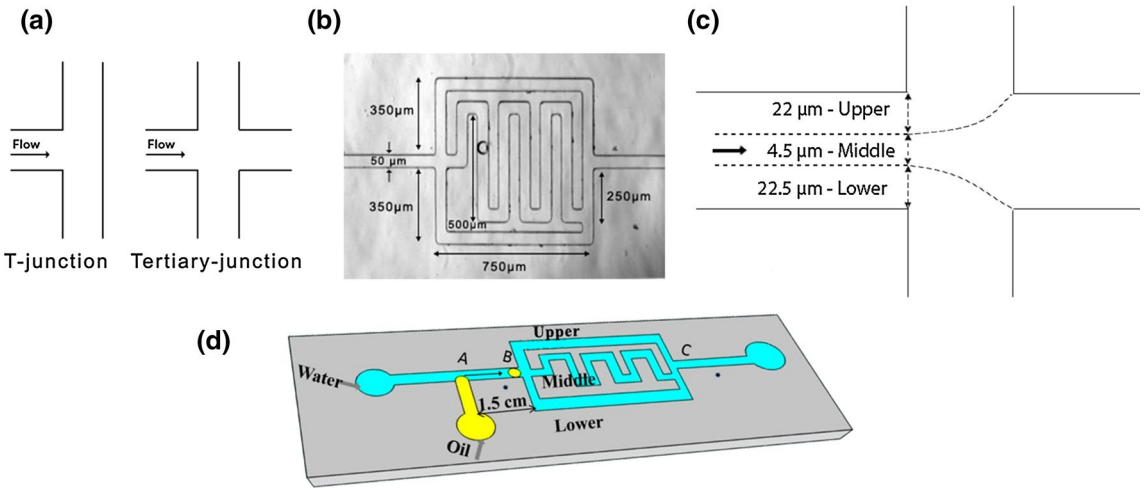

Fig. 1 **a** A schematic comparison of the T-junction vs tertiary junction, **b** an actual optical image of the microchannel network showing a droplet in the middle channel with the highest path length (or, resistance). The respective lengths of the three channel arms were as follows: Upper 1400 μm, Middle 3400 μm and Lower 1150 μm, **c** numerically computed streamline positions for *upper*, *middle* and *lower* channels just before the inlet to the tertiary junction, **d** Layout of the microfluidic chip used in this study showing regions for droplet formation (*point A*; T-junction), droplet monitoring for path selection to upper, middle or lower channels (*point B*; tertiary junction), and droplet exit (*point C*). The T-junction was kept 1.5 cm from the inlet tertiary junction

a laminar, viscous and incompressible flow, the partition of a pressure-driven continuous phase in a rectangular microchannel without any droplet is given by Eq. 1 (refer to SI for analogy between fluidic and electrical parameters; Oh et al. 2012):

$$\Delta P = QR = \frac{12\mu L}{wh^3\left(1-\frac{h}{w}\left(\frac{192}{\pi^5}\sum_{n=1,3,5}^{\infty}\frac{1}{n^5}\tan h\left(\frac{n\pi w}{2h}\right)\right)\right)} \quad (1)$$

This relationship is only valid for Newtonian fluids. Here, L, w and h are the length, width and height of the channel (m), respectively, R is the fluidic resistance (Pa s^3 m^{-1}), Q is the volumetric flow rate (m^3/s), μ is the viscosity (Pa s), and ΔP is the pressure drop (Pa).

It was only recently, experimentally, shown that the path taken by a deformable bubble in a locally asymmetric T-point junction is actually guided by the velocity vectors at the junction and not by the overall resistance of the microchannel (Tan et al. 2008, 2004; Yang et al. 2010). The studies were performed on droplets equal to or greater than the size of the microchannel and, in some cases, to sort two groups of droplets of significantly different sizes. The results illustrated that local variation in channel dimensions can have important implications in the sorting of droplets. In another study, Moon et al. carried out numerical simulations on a vesicle flowing through a symmetric cross-flow tertiary junction (Moon et al. 2014). The size of the vesicle was kept slightly larger than the channel width. The results of this study highlighted that the disperse phase may go into the channel with a higher fluidic resistance at the cost of a lower bending penalty for the vesicle. This phenomenon was explained in terms of a simplified resultant velocity concept and was dominant in the path selection process for low capillary number flows ($Ca_s \leq 0.025$); the resultant velocity hypothesis failed above this value.

Unlike symmetric T-point junctions, the hypothesis of maximum flow rate channel carrying the droplet does not hold true for all cases in symmetric tertiary junctions (Fig. 1a, b). For droplet size of the width of the channel, the partition behavior may be predicted by the resultant velocity at the tertiary junction below a critical Ca_s (Moon et al. 2014). Similarly, a droplet much smaller than the channel size may be expected to follow the streamline passing through its center at low Reynolds number. However, no results have been reported for drops when their size is smaller than the channel size but about the same order. When the size of the droplet is smaller than the channel size but large enough to interact with flow going to different channels following the junction, its path cannot be determined just based on the resultant velocity or the path of the streamline passing through its center. The path taken by the droplet instead depends on many other factors including the position of its center, size, viscosity, flow conditions and the Reynolds number.

In this paper, we consider droplets of size slightly less than the width of the channel and chose flow conditions such that $Ca \ll 1$. The condition on the capillary number ascertains that the droplet does not deform and remains

almost spherical in the microchannel. By performing both experiments and simulations, we systematically investigate the influence of all the operating parameters on the route selection of a single microdroplet in a tertiary junction network. We use oil-in-water as a model system to study the effects of Reynolds number, droplet size and its streamline position, and viscosity of the dispersed phase on the droplet's sorting behavior. Although we approach this problem from a purely fundamental fluid mechanics point of view, the larger motivation to carry out this research work derives from its application in biomedical engineering for sorting CTCs for early cancer screening and theranostics (Karabcak et al. 2014; Shields et al. 2015). The results of this study performed on a single droplet can in future help frame guidelines for selecting appropriate operating conditions to separate a low concentration of abnormal cells (say larger in size, more rigid etc.) from multiple smaller healthy ones given that the physical characteristics of the cell types are known beforehand and the experiments are performed below the critical droplet flow frequency at which the resistance drop due to multiple droplets in a channel does not lead to alteration in final outcomes (Amon et al. 2013).

2 Materials and methods

2.1 System specific details

A network of square cross-sectional microchannels of approx. 50 μm size was prepared using the standard photolithography process (see SI). DI water (18 MΩ cm; Synergy UV, Ultrapure Type-1) was used as the continuous phase, and mineral oil (MO) (kinematic viscosity 34.5 cSt @ 40 °C and density 0.76 g/mL @ 20 °C) or hexadecane (Hex) (kinematic viscosity 2.93 cSt @ 40 °C and density 0.77 g/mL @ 20 °C) (Fischer Scientific) was taken as the disperse phase. The method for precise microdroplet formation at a T-point junction was borrowed from the established protocols in the literature (Yamamoto and Ogata 2013; Tostado et al. 2011; Fu et al. 2010; Li et al. 2012). First, the entire microfluidic chip was primed by flushing with Tween 20 (for $Re = 3$) or sodium dodecyl sulfate (SDS) surfactant (for $Re = 0.3$) (Sigma Aldrich) in water. The priming was done in order to ensure complete wettability of the channels. Next, a single oil emulsion was generated at the T-junction (point A in Fig. 1d) by simultaneous injection of water containing surfactant (same concentration as that used for priming) and oil phase using two separate microcontrolled syringe pumps (Kd Scientific, USA). To generate a single droplet, multiple droplets were formed first followed by a sudden stopping of the oil flow rate which lead to a gradual decrease in the number of droplets in the microchannel all the way down to a single one (in approx. 5–6 s). The droplet size was tuned by varying the flow rate of oil between 0.04 and 0.2 mL/h with respect to water flowing between 0.6 and 0.06 mL/h. 5 w/v % glucose was added to all the experiments performed at $Re = 0.3$ to assist in the smooth movement of larger droplets that otherwise tended to get stuck to the walls. Surfactant concentration was kept sufficiently high in all the experiments, larger than the critical micellar concentration (cmc) value, to maintain the surface tension constant.

2.2 Experimental measurements

The freely navigating droplets were monitored downstream at point B (Fig. 1d) using an Olympus BX53 optical microscope fitted with a CMOS digital camera (Orca Flash 4.0 V2, Hamamatsu). Time-lapsed images of the droplets were acquired at 100 fps, 5-ms exposure and 1 px = 2 μm resolution and later analyzed using the open-source ImageJ software (1.47t). All experiments were performed once the continuous phase reached a steady state.

The viscosity measurements were taken on a fully automatic plate MCR rheometer (Anton Paar, Austria). The measurements were made in a parallel-plate spindle by applying shear rates between 0.1 and 800 s^{-1}. The interfacial properties were determined using a programmable plate tensiometer (Kruss 100, Germany).

2.3 Numerical approach

During the last two decades, the lattice Boltzmann modeling (LBM) has become a popular choice for solving problems involving interfacial dynamics and complex boundaries (Shi et al. 2014; Yan et al. 2012). This model is easy to implement due to its construction based on simplified kinetic models that incorporate the essential physics of microscopic or mesoscopic process such that the averaged macroscopic properties obey macroscopic equations. The kinetic theory introduces two distinct features to the LBM from other numerical schemes. First, the phase space in the LBM is linear. Simple streaming and collision processes combine to allow recovery of nonlinear macroscopic advection. Second, the pressure term in the LBM is solved using equation of state which has great advantage over traditional numerical schemes where the pressure is solved using Poisson's equations and often produces numerical difficulties. In addition, the LBM produces the interface inherently getting rid of complex interface tracking and grid generation techniques near the interface that are required in traditional numerical approaches.

2D lattice Boltzmann simulations were performed to mimic the experiments using the grid size of 1580 × 730 lattice units (LU). The width of the channel was taken as 50

LU. An oil droplet was initially placed at a distance of 300 LU from the tertiary junction using water as the continuous phase. The boundary conditions at the inlet and outlet of channel were of constant velocity condition. The experimental conditions in the present simulations were replicated by scaling 1 lattice unit as 1 μm and 1 lattice time as 2.58E − 4 μs. The density of all the phases was assumed to be the same. Full details of the numerical method are given in the SI.

3 Results

3.1 Streamline position of the microdroplet

The path selected by a microdroplet was defined according to its streamline position in the inlet channel just before entering the tertiary junction. For this, the inlet channel was divided into three sections based on the downstream flow division of the continuous phase into the upper, middle and lower channels. The width of each section was determined numerically using LBM as 22, 4.5 and 22.5 μm for upper, middle and lower channels, respectively, assuming for simplicity the velocity profile of only the continuous phase inside a 2D square channel (Fig. 1c). We limited our study to 2D simulations to qualitatively understand the effect of inertial and drag forces on the droplet sorting since the computational costs of performing 3D simulations for all the cases were quite large.

In experiments, the single droplet formation took place at a T-junction far away from the point of analysis. This approach, although simple, had one limitation that it led to poor control on the exact position of the microdroplet in the streamline as it entered the tertiary junction. For more precise formation, channel-integrated microfluidic valves may be used (Jeong et al. 2016; Churski et al. 2010). Once the droplet was formed, it continued to follow its streamline without any vertical deviation. To overcome the limitation of poor position control, a large number of experiments were performed to get a statistical pool of data points from which a particular trend could be formulated. We observed that there was a higher propensity of the droplets to form on the same side as that of the T-junction (kept lower and 1.5 cm away from the inlet tertiary junction as shown in Fig. 1d) especially for larger droplets. For instance, at *Re* equal to 0.3, approximately 85% of the droplets formed between the sizes 30 to 45 μm (out of a total of 13) were found to lie in the middle and lower zone. Therefore, for purposes of this study, we focused only on the droplet transitions made from middle to lower channels, expecting the findings to be equally applicable for transitions on the upper side. Furthermore, simulations gave us the freedom to choose any droplet streamline location for further verification.

3.2 Effect of droplet size at different Reynolds numbers

The net forces acting on a droplet inside a microjunction vary as a function of its size which influences its overall navigation behavior. To study this effect, experiments were performed with mineral oil (MO) droplets in water. The droplet size was coarsely varied by changing the velocity of the MO at the T-junction where the droplet was formed. As the velocity of the dispersed phase was increased, the volume of oil sheared by the continuous phase also became higher resulting in droplets of bigger sizes. The maximum value of capillary number calculated for these experiments was 0.007. Capillary number was defined with respect to the continuous phase only. As a result, all the droplets of size less than or equal to the width of channel showed minimal deformation and appeared spherical in shape. The continuous phase velocity was then systematically increased to study the effect of Reynolds number, defined with respect to the continuous phase taking the width of the channel as the characteristic length.

At $Re = 3$ For both experiments and numerical simulations, the position of the droplet at the tertiary junction was plotted as a function of the droplet size and the outcome of the path selection (Fig. 2). It was observed that for all droplet sizes varying from 25 to 50 μm, droplets lying in the middle zone always opted for the middle channel and similarly, droplets with streamline position in the lower zone, went into the lower channel. These results suggested that the path selection at this Reynolds number was mainly driven by inertial forces. To confirm that the results are truly due to inertial effects, additional simulations were performed at $Re = 30$. At this condition, droplets in the lower streamline also migrated into the middle channel although they were highly deformed due to the high shear stress (Ca = 0.07) (see Fig. S2 and video v1).

At $Re = 0.3$ When the *Re* number was reduced ten times to 0.3, inertia no longer remained the most dominant force in the path selection process. The experimental results showed that for a small range between 41 and 45 μm, the droplets entering through the middle zone still went into the lower channel (Fig. 2). This was attributed to the higher effective drag force on the lower part of the droplet above a critical size. Beyond 45 μm, the droplet again selected the middle channel based on the resultant velocity hypothesis as its center again rested in the middle zone. Both the experimental and numerical simulation results demonstrated good similarity highlighting the accuracy of the procedures.

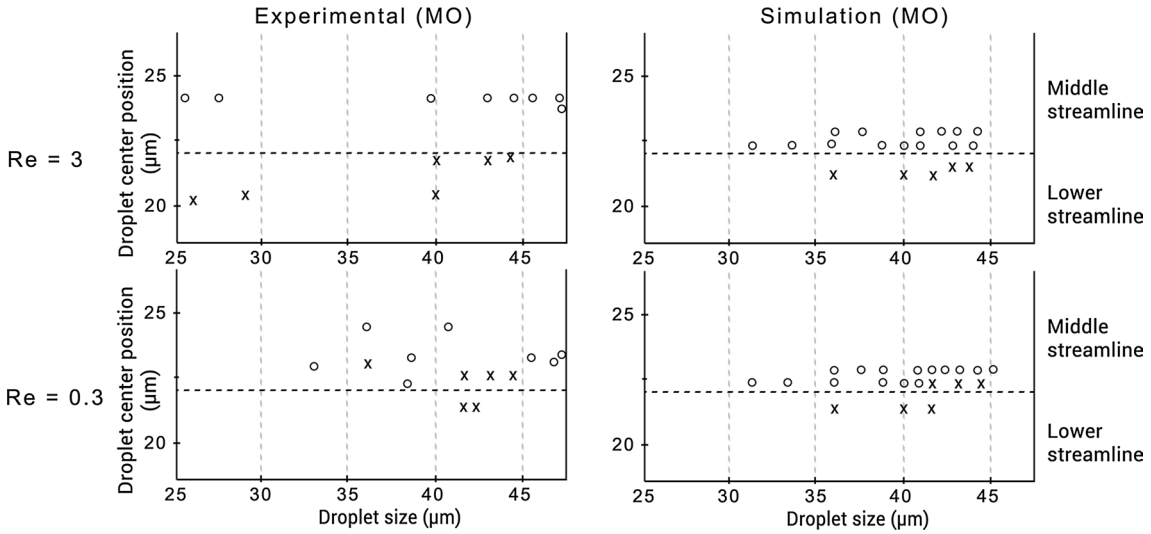

Fig. 2 Experimental and simulation results for droplet size versus center position showing path selected by the droplet at Re = 3 and 0.3. The *circles* represent the selection of middle channel and crosses imply the selection of lower channel

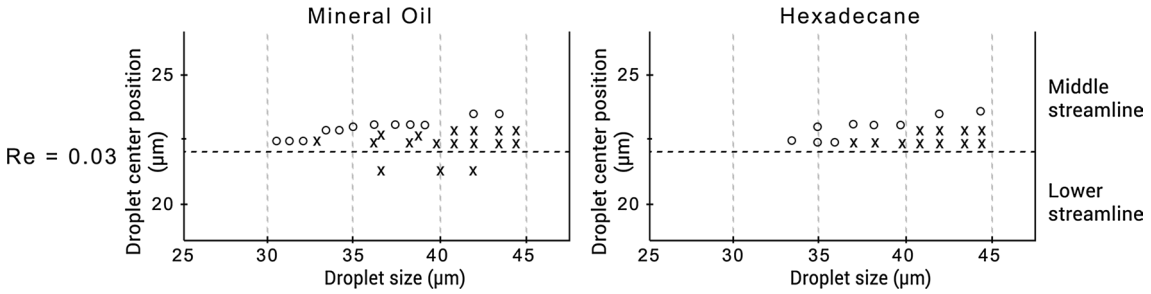

Fig. 3 Simulations at $Re = 0.03$ for **a** mineral oil and **b** hexadecane showing effects of both droplet size and viscosity on the path selection process. The *circles* represent the selection of middle channel and crosses imply the selection of lower channel

At $Re = 0.03$ When the *Re* number was further decreased to 0.03, simulations showed that the critical droplet size required for transition from middle to lower channel reduced to 33 μm, thereby increasing the overall size range of the transformation regime (Fig. 3a and videos v2 and v3). The transformation region also widened in the vertical direction in a size-dependent manner, i.e., the same size droplet opted for the middle path for a much wider set of distances extending toward the center of the channel. The simulation results could not be verified by actual experiments due to the setup limitations for performing experiments at such low *Re*.

3.3 Effect of viscosity

To study the effect of viscosity on the path selection process, simulations were repeated at *Re* 0.03 using a lower viscosity oil, Hex, in place of MO as the dispersed phase. The interfacial tension value of 9.5 mN/m, corresponding to that between MO and 0.5 w/v % Tween 20, was kept constant in the study with Hex. With a higher viscosity droplet, the transition region was wider, giving a smaller critical diameter for going to the lower channel similar to the *Re* equal to 0.03 case discussed above (Fig. 3b). Also, the width of the transition region was slightly higher in the vertical direction in the case of MO as compared to Hex. Simulations performed for *Re* 3 and 0.3 showed no major variations due to change in viscosity (Fig. S3).

3.4 Effect of interfacial tension

Interfacial tension is an important parameter for ensuring droplet formation, shape and stability. Since the interfacial tension acts uniformly along a spherical droplet, it is not expected to impart any directional force since the capillary number is quite low in our experiments. Nevertheless, in a dynamic system such as ours, it is important to ensure that

there is minimal lateral diffusion of the surfactants under shear flow as this may cause local interfacial force gradients to form on the surface of the droplet, affecting the overall selection process. One way to avoid this is to have a complete surface coverage of all the interfaces by the surfactant.

We estimated the interfacial tension saturation limit of surfactant concentration in our system using a Wilhelmy plate tensiometer. For this, Tween 20 was taken in varying amounts in a fixed volume of water and the interfacial properties were measured against both MO and Hex at each concentration (Fig. S4). The interfacial tension was observed to decrease monotonically with increasing surfactant concentration and gradually became constant at approx. 9.5 mN/m corresponding to 0.5 w/v % of Tween 20 in case of MO and 0.1 w/v % in case of Hex. The exposed surface area to volume ratio in the tensiometer was then normalized to that of our experimental setup (see Fig. S5 and SI). The two surface areas to volume ratios almost matched each other so the final surfactant concentrations used in our experiments were also kept the same as above. Also, to further check the validity of our findings, a few random experiments were performed with different Tween 20 concentrations using Hex droplets of sizes equal to the width of channel. The results showed no variation in the path selection properties (Fig. S6) establishing that interfacial tension indeed does not play a role in the path selection process in our experiments. Amounts used for SDS were approximately doubled since the topological cross-sectional area of SDS molecules (74.8 $Å^2$) is roughly half of that of Tween 20 (133 $Å^2$) (National Center for Biotechnology Information 2015; National Center for Biotechnology Information. PubChem Compound Database and CID = 34 2326).

4 Discussion

The tertiary junction in our microfluidic network divides the liquid into three branches; the flow rates of which are proportional to the resistance of each channel. At low Re, if the size of the drop is much smaller than the size of the microchannel, then the droplet follows the path of its center's streamline. If the size of the droplet is equal to or larger than the size of the channel, then the droplet follows the resultant velocity direction at the junction (Moon et al. 2014). We work in the intermediate droplet size regime where different regions of the droplet experience forces toward the different flow directions at the junction (Fig. 4a). As a result, the direction chosen by the droplet is not simply determined by its streamline as in the case for small size droplets or the resultant velocity direction as is the case for large droplets. Away from the junction, the droplet has zero velocity in the y direction (Mortazavi and Tryggvason 2000); however, as it approaches the junction, the droplet moves into any particular channel depending on the shear forces experienced by the droplet and the inertial forces acting along the flow direction (Fig. 4a). The viscous drag forces acting on the particle tend to guide it along the streamlines, whereas the inertial force tends to move it along its direction of motion. In general, the droplet at high flow rates has a tendency to continue moving in its original direction along the fluid flow due to inertia, and the shear stresses acting on the sides can drag the droplet into the channel away from the flow direction depending on the net sum of the viscous forces generated by the daughter flows (in channels B and C in our case).

To determine the preferred path chosen by the droplet in our experiments, we took a ratio of the response time of the droplet due to the resulting shear and inertial forces in the vertical and the horizontal directions, respectively. If the time taken for the center of the droplet to cover the distance to the lower wall (τ_{shear}) was less than the time taken for it to pass through the junction due to its momentum (τ_{inertial}), the droplet was said to choose the vertical path and vice versa. For τ_{inertial} (Eq. 2), the droplet velocities were estimated at the start of the junction (v_{d1}) and at the start of the channel A (v_{d2}) by using the relation between the droplet velocity at any time and the maximum flow velocity provided by Hetsroni and Haber for Poiseuille flow (Hetsroni and Haber 1970).

$$\tau_{\text{inertial}} = \frac{2H}{v_{d1} + v_{d2}} \tag{2}$$

Here, H is the half channel height. The τ_{shear} was obtained by writing the force balance equation in the y direction. For a droplet of radius r,

$$\frac{4\pi r^3}{3}\rho_{\text{d}}\frac{\text{d}^2 y}{\text{d}t^2} = F_{\text{s}} \tag{3}$$

where F_{s} is the total shear force acting on the particle and ρ_{d} is the density of the droplet. Assuming F_{s} to be constant during the motion of the droplet at the junction, if the distance between the droplet center and the lower wall is '$r + h$' (Fig. 4a), the time taken (τ_{shear}) by the droplet center to cover this distance is,

$$\tau_{\text{shear}} = \sqrt{\frac{r+h}{F_{\text{s}}/m}} \tag{4}$$

where h is the distance between the lower wall and the droplet edge. The shear stress (F_{B}) generated by the flow going to channel B tries to drag the particle in the $-y$ direction, whereas the stress generated (F_{c}) by flow going to the

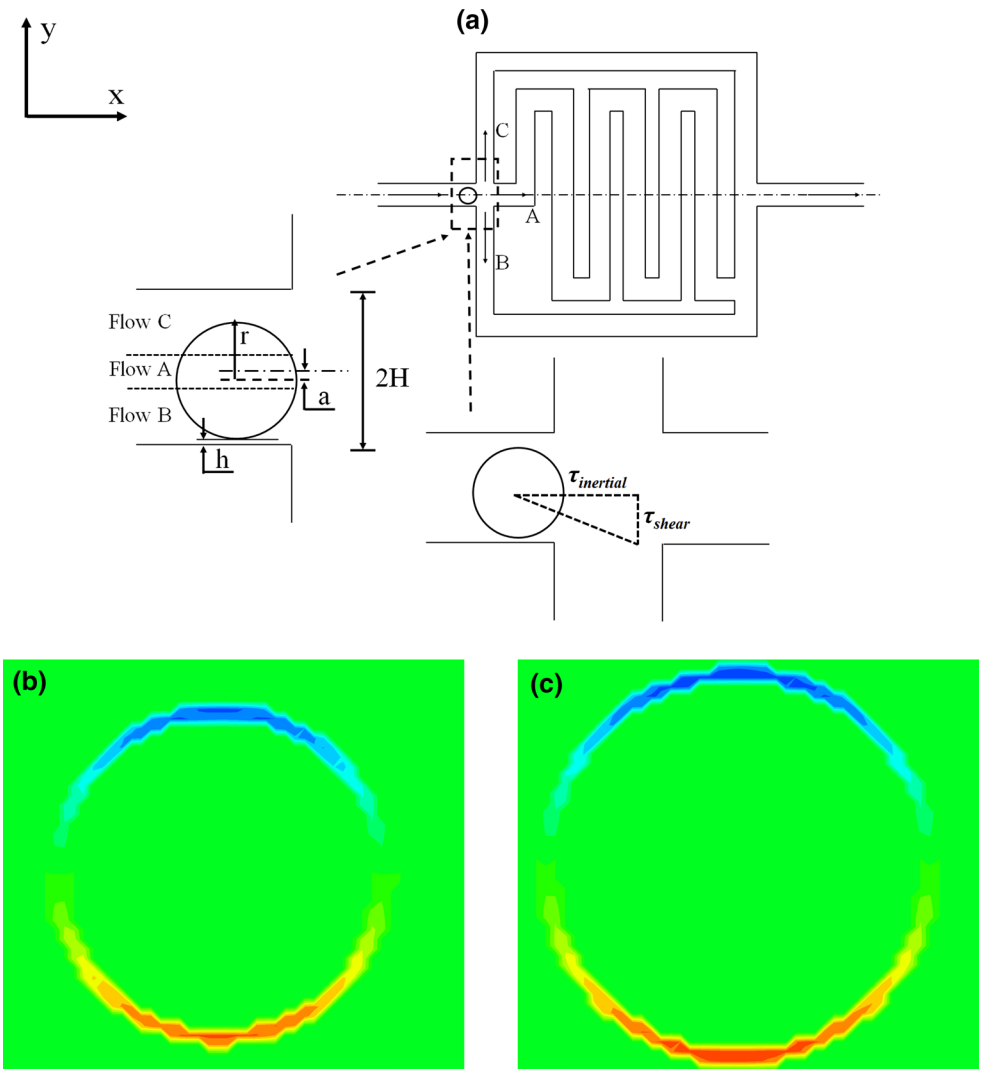

Fig. 4 **a** Schematic of force balance analysis on a microdroplet inside a tertiary-junction microchannel. **b** and **c** The *contour plots* indicate shear stresses acting on mineral oil droplets of sizes 36 μm (**b**) and 42 μm (**c**), where the minimum and maximum stress values correspond to −120 N/m2 (*blue*) and 120 N/m2 (*red*), respectively (color figure online)

upper channel C tries to drag the particle in the $+y$ direction. The forces acting on the particle due to these two stresses can be written as

$$F_B = \sigma_B A_B \tag{5}$$

$$F_C = \sigma_C A_C \tag{6}$$

where σ_B and σ_c are the stresses pulling the droplet in the $-y$ and $+y$ directions, and A_B and A_c are the respective areas over which these stresses act. The total shear force acting on the particle is thus $F_S = F_B - F_C$ in the direction of the downward channel (−y). The shear stress acting on the particle is proportional to the shear rate and the viscosity (μ_c) of the continuous phase. The shear rate in turn is proportional to the particle velocity (v) and the inverse of the gap between the particle interface and the wall. The stress on the lower interface is given by

$$\sigma_B \sim \mu_c v/h \tag{7}$$

For a constant droplet size, as the distance (h) between the wall and the drop decreases, the lubrication stress on the particle increase. Also, the area A_B over which the stress acts also increases. Hence, the total shear force, F_S, increases and time τ_{shear} decreases with lowering of the distance between the droplet and the lower wall. On the other hand, $\tau_{inertial}$ remains more or less constant. In Figs. 2 and 3, for the same drop size, as the droplet moves closer to the lower wall below a critical distance, it always goes to the lower channel. Also for the same distance (h) between the wall and the droplet, as the size (or mass) of the droplet increases, τ_{shear} is expected to increase as well from Eq. 4 or in other words, above a critical size, the droplet is expected to go to the middle channel.

The viscous stress estimate from Eq. 7 assumes the droplet to be of very high viscosity compared to the continuous phase. As the viscosity of the dispersed phase decreases (in comparison to that of the continuous phase), the droplet rotates faster and the shear stress acting on it

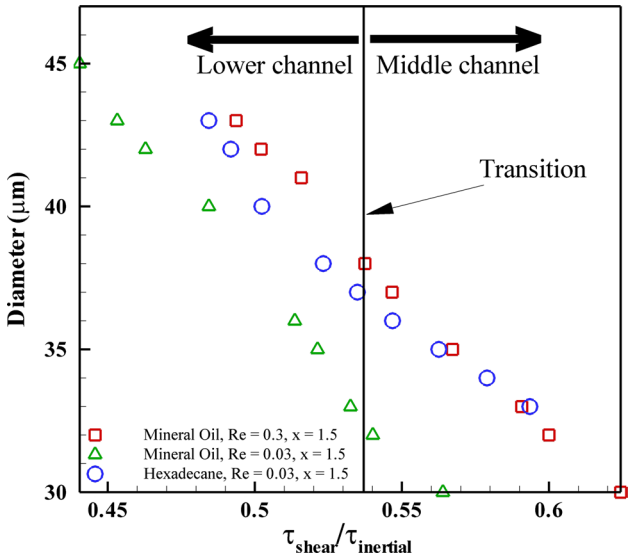

Fig. 5 Response time ratio (RTR) of shear to inertial forces acting on the droplet at the junction. The *line* indicates transition in the droplet trajectory from lower to middle channel

decreases (Ma et al. 2014). So under similar conditions, one would expect the higher viscosity mineral oil drops to move to the lower channel at a smaller size. Simulation results shown in Fig. 3 agree with this prediction where for the same size, droplets start transitioning to the lower channel at larger distances from the lower wall. The sorting of droplets based on the size has been achieved in the past in T-junction microchannels (Tan et al. 2008). Tertiary-junction channels like the ones used in this work can be used to sort same size droplets or particles based on their density and viscosity.

LBM simulations were performed to determine F_s acting on the droplet as it entered the junction, and τ_{shear} was calculated using Eq. 4. The shear stress produced on 35 and 42 μm size droplets at $Re = 0.3$ and $a = 1.5$ μm are shown in Fig. 4b. The color contour plots clearly indicate that the 42 μm diameter droplet has a greater stress due to the larger lubrication forces generated between the droplet–wall interface.

When we plotted the droplet size as a function of response time ratio (RTR) $\tau_{shear}/\tau_{inertial}$ for MO at $Re = 0.3$, 0.03 and Hex at $Re = 0.03$, we found that the transition of droplets for each case occurred at $\tau_{shear}/\tau_{inertial} \sim 0.535$ (Fig. 5). The center of the droplets was placed 1.5 μm below the center of the channel in each case. The droplets with RTR > 0.535 were observed to travel in channel A and others in channel B. These results suggest that the resultant shear and inertial forces are important factors in the transition of droplets from channel A to channel B. It should be noted that the dynamic nature of the droplets can continuously change the forces acting on them which are not considered in the present analysis. This could be a possible reason for the transition of droplets being observed at RTR equal to 0.535 instead of 1. Since the droplets, however, under different conditions follow the same transition pattern and RTR value, it gives us a good physical understanding of the forces and a unifying approach to characterize the sorting of droplets inside a tertiary-junction microchannel. The velocities obtained from our model are in the limit of the velocities obtained from the simulations as well as the measured velocities of the continuous phase alone (see SI). In future, more rigorous mathematical approaches may be undertaken for full analysis.

5 Conclusions

We demonstrated the ability of tertiary-junction microchannel networks to sort droplets according to physical properties. There is a clear droplet size about which the path selected by the droplet changes. The experiments and simulations performed on droplets of MO and Hex show the transition of droplets at different diameters. To observe the effect of shear forces and inertial forces acting on the droplet at the junction, we calculated the response time ratios of $\tau_{shear}/\tau_{inertial}$ and found that the transition of both MO and Hex droplets occurs at time response ratio of 0.535. The time response ratio indicates that the physical nature of shear forces and inertial forces are responsible for occurrence of transition at the tertiary junction. Interfacial tension does not show any effect on droplet navigation behavior. Thus, a combination of these physical properties can be used to sort droplet according to the required parameters. Our claims, however, are made only in the limit where the droplets do not deform and the Capillary number is low. An undergoing numerical study will be help us to design optimized experimental conditions and network design for any desired sorting application.

Acknowledgements We thank the Asian Office of Aerospace Research and Development (AOARD, Grant No. FA2386-15-1-4031) for providing the necessary funds to carry out this research. We are grateful to Prof. Rajesh Khanna for helping with the tensiometer experiments. SK acknowledges his DST INSPIRE fellowship.

References

Amon A, Schmit A, Salkin L, Courbin L, Panizza P (2013) Path selection rules for droplet trains in single-lane microfluidic networks. Phys Rev E 88:013012

Baroud CN, Gallaire F, Dangla R (2010) Dynamics of microfluidic droplets. Lab Chip 10:2032–2045

Belloul M, Courbin L, Panizza P (2011) Droplet traffic regulated by collisions in microfluidic networks. Soft Matter 7:9453–9458

Bruus H (2007) Theoretical microfluidics. OUP Oxford, Oxford

Choi W, Hashimoto M, Ellerbee AK, Chen X, Bishop KJM, Garstecki P, Stone HA, Whitesides GM (2011) Bubbles navigating through networks of microchannels. Lab Chip 11:3970–3978

Christopher GF, Noharuddin NN, Taylor JA, Anna SL (2008) Experimental observations of the squeezing-to-dripping transition in T-shaped microfluidic junction. Phys Rev E 78:036317

Churski K, Michalski J, Garstecki P (2010) Droplet on demand system utilizing a computer controlled microvalve integrated into a stiff polymeric microfluidic device. Lab Chip 10:512–518

Doh I, Erdem EY, Pisano AP (2012) Trapping and collection of uniform size droplets using a well array inside a microchannel. In: IEEE 25th International Conference Micro Electro Mechanical Systems, pp. 1113–1116

Fu T, Ma Y, Funfschilling D, Zhu C, Li HZ (2010) Squeezing-to-dripping transition for bubble formation in a microfluidic T-junction. Chem Eng Sci 65:3739–3748

Garstecki P, Fuerstman MJ, Stone HA, Whitesides GM (2006) Formation of droplets and bubbles in a microfluidic T-junction scaling and mechanism of break-up. Lab Chip 6:437–446

Glawdel T, Elbuken C, Ren CL (2012) Droplet formation in microfluidic T-junction generators operating in the transitional regime I experimental observations. Phys Rev E 85:016322

Hetsroni G, Haber S (1970) The flow in and around a droplet or bubble submerged in an unbound arbitrary velocity field. Rheol Acta 9:488–496

Huebner A, Bratton D, Whyte G, Yang M, Demello AJ, Abell C, Hollfelder F (2009) Static microdroplet arrays: a microfluidic device for droplet trapping, incubation and release for enzymatic and cell-based assays. Lab Chip 9:692–698

Husny J, Cooper-White JJ (2006) The effect of elasticity on drop creation in T-shaped microchannels. J Non-Newton Fluid Mech 137:121–136

Jeong H-H, Lee B, Jin SH, Jeong S-G, Lee C-S (2016) A highly addressable static droplet array enabling digital control of a single droplet at pico-volume resolution. Lab Chip 16:1698–1707

Jousse F, Farr R, Link DR, Fuerstman MJ, Garstecki P (2006) Bifurcation of droplet flows within capillaries. Phys Rev E 74:036311

Karabcak NM et al (2014) Microfluidic, marker-free isolation of circulating tumor cells from blood samples. Nat Protocol 9:694–710

Lee YW (2013) Novel design of integrated microfluidic thermal system with self-assembling magnetic particles for electronic cooling. Microelectron Eng 111:285–288

Li XB, Li FC, Yang JC, Kinoshita H, Oishi M, Oshima M (2012) Study on the mechanism of droplet formation in T-junction microchannel. Chem Eng Sci 69:340–351

Link DR, Anna SL, Weitz DA, Stone HA (2004) Geometrically mediated breakup of drops in microfluidic devices. Phys Rev Lett 92:054503

Liu H, Zhang Y (2009) Droplet formation in a T-shaped microfluidic junction. A Phys 106:034906

Ma S, Sherwood JM, Huck WTS, Balabani S (2014) On the flow topology inside droplets moving in rectangular microchannels. Lab Chip 14:3611–3620

Moon JY, Kondaraju S, Choi W, Lee JS (2014) Lattice Boltzmann-immersed boundary approach for vesicle navigation in microfluidic channel networks. Microfluid Nanofluidics 17:1061–1070

Mortazavi S, Tryggvason G (2000) A numerical study of the motion of drops in Poiseuille flow. Part 1. Lateral migration of one drop. J Fluid Mech 411:325–350

Mugele F, Duits M, Ende DVD (2010) Electrowetting: a versatile tool for drop manipulation, generation and characterization. Adv Colloid Interface Sci 161:115–123

National Center for Biotechnology Information. PubChem Compound Database; CID = 3423265. https://pubchem.ncbi.nlm.nih.gov/compound/3423265. Accessed 29 Sept 2015

National Center for Biotechnology Information. PubChem Compound Database; CID = 443314. https://pubchem.ncbi.nlm.nih.gov/compound/443314. Accessed 29 Sept 2015

Niu X, Gulati S, Edel JB, deMello AJ (2008) Pillar-induced droplet merging in microfluidic circuits. Lab Chip 8:1837–1841

Oh KW, Lee K, Ahn B, Furlani EP (2012) Design of pressure-driven microfluidic networks using electric circuit analogy. Lab Chip 12:515–545

Sang L, Hong Y, Wang F (2009) Investigation of viscosity effect on droplet formation in T-shaped microchannels by numerical and analytical methods. Microfluid Nanofluidics 6:621–635

Schindler M, Ajdari A (2008) Droplet traffic in microfluidic networks: a simple model for understanding and designing. Phys Rev Lett 100:044501

Sessoms DA, Belloul M, Engl W, Roche M, Courbin L, Panizza P (2009) Droplet motion in microfluidic networks: hydrodynamic interactions and pressure-drop measurements. Phys Rev E 80:016317

Shi Y, Tang GH, Xia HH (2014) Lattice Boltzmann simulation of droplet formation in T-junction and flow focussing devices. Comput Fluids 90:155–163

Shields CW, Reyes CD, Lopez GP (2015) Microfluidic cell sorting: a review of the advances in the separation of cells from debulking to rare cell isolation. Lab Chip 15:1230–1249

Tan YC, Fisher JS, Lee AI, Cristini V, Lee AP (2004) Design of microfluidic channel geometries for the control of droplet volume, chemical concentration, and sorting. Lab Chip 4:292–298

Tan YC, Ho YL, Lee AP (2008) Microfluidic sorting of droplets by size. Microfluid Nanofluidics 4:343–348

Teh SY, Lin R, Hung LH, Lee AP (2008) Droplet microfluidics. Lab Chip 8:198–220

Tostado CP, Xu J, Luo G (2011) The effects of hydrophilic surfactant concentration and flow ratio on dynamic wetting in a T-junction microfluidic device. Chem Eng J 171:1340–1347

Velev OD, Prevo BG, Bhatt KH (2003) On-chip manipulation of free droplets. Nature 426:515–516

Xu JH, Li SW, Tan J, Luo GS (2008) Correlations of droplet formation in T-junction microfluidic devices: from squeezing to dripping. Microfluid Nanofluidics 5:711–717

Yamamoto K, Ogata S (2013) Effects of T-junction size on bubble generation and flow instability for two phase flows in circular microchannels. Int J Multiph Flow 49:24–30

Yan Y, Guo D, Wen SZ (2012) Numerical simulation of junction point pressure during droplet formation in a microfluidic T-junction. Chem Eng Sci 84:591–601

Yang CG, Xu ZR, Wang JH (2010) Manipulation of droplets in microfluidic systems. TrAC Trends Anal Chem 29:141–157

Zakinyan A, Nechaeva O, Dikansky Y (2012) Motion of a deformable drop of magnetic fluid on a solid surface in a rotating magnetic field. Exp Therm Fluid Sci 39:265–268